AIP Journal of Applied Physics

Electron scattering mechanisms in Cu-Mn films for interconnect applications

F. Misják, K. H. Nagy, P. Lobotka, and G. Radnóczi

Citation: Journal of Applied Physics **116**, 083507 (2014); doi: 10.1063/1.4893718
View online: http://dx.doi.org/10.1063/1.4893718
View Table of Contents: http://scitation.aip.org/content/aip/journal/jap/116/8?ver=pdfcov
Published by the AIP Publishing

Articles you may be interested in

Study of adhesion and chemical bonds in the reaction layer formed at Cu-Mn interconnection/SiO2 interface
J. Appl. Phys. **113**, 174902 (2013); 10.1063/1.4803500

An investigation of optimal interfacial film condition for Cu-Mn alloy based source/drain electrodes in hydrogenated amorphous silicon thin film transistors
AIP Advances **2**, 022147 (2012); 10.1063/1.4727939

Diffusion barrier properties of amorphous and nanocrystalline Ta films for Cu interconnects
J. Appl. Phys. **106**, 113513 (2009); 10.1063/1.3266164

Resistivity reduction by external oxidation of Cu–Mn alloy films for semiconductor interconnect application
J. Vac. Sci. Technol. B **27**, 1963 (2009); 10.1116/1.3179167

On the use of alloying elements for Cu interconnect applications
J. Vac. Sci. Technol. B **24**, 2485 (2006); 10.1116/1.2357744

AIP Journal of Applied Physics

Journal of Applied Physics is pleased to announce André Anders as its new Editor-in-Chief

[This article is copyrighted as indicated in the article. Reuse of AIP content is subject to the terms at: http://scitation.aip.org/termsconditions. Downloaded to] IP: 148.6.78.172 On: Thu, 04 Sep 2014 14:30:22

JOURNAL OF APPLIED PHYSICS 116, 083507 (2014)

Electron scattering mechanisms in Cu-Mn films for interconnect applications

F. Misják,[1] K. H. Nagy,[1] P. Lobotka,[2] and G. Radnóczi[1]
[1]Research Centre for Natural Sciences, Hungarian Academy of Sciences, H-1525 Budapest, P.O. Box 49, Hungary,
[2]Institute of Electrical Engineering, Slovak Academy of Sciences, Dúbravská cesta 9, 841 04 Bratislava, Slovak Republic

(Received 3 June 2014; accepted 11 August 2014; published online 25 August 2014)

Electrical properties and corresponding structural features of Cu-Mn alloy films with potential application as barrier and interconnect layers were studied. Cu-Mn films were deposited by DC magnetron sputtering at room temperature on SiO_2 substrates. Electrical resistivity measurements were made as a function of film composition and temperature. The specific resistivity varies linearly with the Mn content showing a maximum of 205 $\mu\Omega$cm at 80 at. % Mn. The temperature coefficient of resistance (TCR) of all alloy films is low, showing non-metallic conductivity for most compositions. Also a minimum TCR has been observed in the 40–80 at. % Mn range which was attributed to a magnetic transformation around 200–300 K. Electrical resistivity measurements are correlated with the film structure revealed by transmission electron microscopy to clarify the phase regions throughout the composition range. In the 20–40 at. % and 70–80 at. % Mn ranges, two-phase structures were identified, where Cu- or Mn-rich solid solution grains were surrounded by a thin amorphous covering layer. Based on the revealed phase regions and morphologies electron scattering mechanisms in the system were evaluated by combining the Matthiessen's rule and the Mayadas-Schatzkes theory. Grain boundary reflectivity coefficients ($r = 0.6$–0.8) were calculated from fitting the model to the measurements. The proposed model indicates that, in a binary system, the special arrangement of the two phases results in new scattering mechanisms. The results are of value in optimizing the various parameters needed to produce a suitable barrier layer.
© 2014 Author(s). All article content, except where otherwise noted, is licensed under a Creative Commons Attribution 3.0 Unported License. [http://dx.doi.org/10.1063/1.4893718]

I. INTRODUCTION

In advanced semiconductor technology, copper is the material of transistor contacts and interconnects. The high diffusion rate for copper in silicon and silicon-oxides has required the application of diffusion barriers. As the semiconductor industry moves beyond the 30 nm technology, there will be a need to reduce the barrier width below 4 nm while retaining its diffusion integrity and adhesion properties. One possible way for reaching this dimension can be the utilization of self-organised processes to form conformal barrier layers in interconnect structures. Metallization by alloying an appropriate element with Cu which could segregate to the Cu/dielectric interface during subsequent annealing can be a promising solution for this requirement. Among various alloying elements Mn has been reported to form a reliable uniform barrier layer.[1–7]

Beside the barrier-forming ability of Cu-Mn alloys, electrical resistivity, adhesion and surface properties are of importance as well. Though several studies have been made on the self-forming barrier process, few of these focused on the electrical characteristics of the Cu alloy films.[8,9] During the segregation of Mn from the Cu-Mn alloy to the interfaces the composition and resistivity of layers varies determining the properties of the interconnects formed. Mapping the whole Cu-Mn system will provide a fundamental understanding and assist in the search for optimum parameters for future technological development.

The authors previously investigated the composition dependence of structure and phases of 50 nm thick Cu-Mn films.[10] Plan-view TEM and SAED revealed deviations from the equilibrium phase diagram at room temperature. Three single-phase composition intervals have been identified. In the low Mn content region, below 35 at. % Mn, a Cu-based fcc solid solution was found. Around 50 at. % Mn content the films had a homogeneous low-contrast appearance which indicated an amorphous structure. In the high Mn content zone, around 100 at. %, an α-Mn based solid solution was identified. Based on the topological rules of phase diagrams, it can be concluded that the three single-phase regions must be separated by two two-phase transition regions. However, mapping of these transition zones was not a straightforward matter since detection of an amorphous material as a second, minority phase between crystalline grains is a difficult task.

Electrical conductivity measurements are an effective tool for characterization of alloy films. Besides measuring conductivity, the electrical properties also carry information about the phase state of the alloys. Evaluating the phases and morphologies in the system can also help in determining the electron scattering mechanisms providing essential information for applications. Mayadas-Shatzkes proposed a model[11] which correlates morphology with scattering mechanisms influencing the film resistivity. According to the model, three main scattering mechanisms are simultaneously operating in a thin film system: (i) thermal, (ii) grain boundary, and (iii) external surface scattering. Other mechanisms (e.g., solute scattering) can be added to describe completely the resistivity of the alloy films.

 © Author(s) 2014

[This article is copyrighted as indicated in the article. Reuse of AIP content is subject to the terms at: http://scitation.aip.org/termsconditions. Downloaded to] IP: 148.6.78.172 On: Thu, 04 Sep 2014 14:30:22

In this paper, we report resistivity measurements made over the whole composition range of the Cu-Mn films. The implications from these electrical measurements are correlated with the film structure studied by transmission electron microscopy (TEM) in order to investigate the scattering mechanisms, phase state and also the transitions between phase regions.

II. EXPERIMENTAL

Cu-Mn alloy films were co-deposited in an ultra-high-vacuum DC magnetron sputtering system. The targets of Cu and Mn (of 99.99% and 99.95% purity, respectively) were mounted 25° towards the vertical and the rotating substrate holder was positioned 12 cm from them. Cu-Mn thin films of 1 μm thickness were grown at room temperature on oxidized (100) silicon wafers. Prior to deposition the sputtering chamber was evacuated to 5×10^{-6} Pa base pressure after which Ar (99.999 % purity) was introduced to a pressure of 2×10^{-1} Pa. The targets were pre-sputtered before deposition with shutters closed for 5–10 min. Magnetron powers were adjusted between 0 and 110 W and the deposition rate of the layers was 0.4 nm/s. The resulting series of samples covered the whole composition range in 10 at. % steps of Mn concentration. The compositions as a function of the magnetron powers (P) are shown in Fig. 1.

Electrical resistivity measurements were performed by the standard van der Pauw method. The temperature dependence of the film resistance (R(T)) was measured in a cryostat. An AC bridge LR-700 (Linear Research) was used for precise measurement of the resistance in the temperature range of 80–320 K. First, the samples were cooled to ~80 K then the temperature was gradually raised to 320 K. The samples were heated in vacuum $\sim 10^{-1}$ Pa at a rate of 1 K/min. All the R(T) dependences were numerically differentiated in order to obtain the temperature dependence of the temperature coefficient of resistance $TCR = 1/R \times dR/dT$.

Structural characterization was carried out by conventional transmission electron microscopy using a Philips CM-20 microscope at 200 keV. The cross-sectional TEM specimens were prepared by mechanical polishing and Ar ion-milling. Special Ti supporting discs[12] were used to embed the samples and protect them from heat load during thinning. In order to verify the composition of samples, analytical measurements were made using a Ge detector (NORAN Energy Dispersive Spectrometer system) attached to the CM-20 microscope.

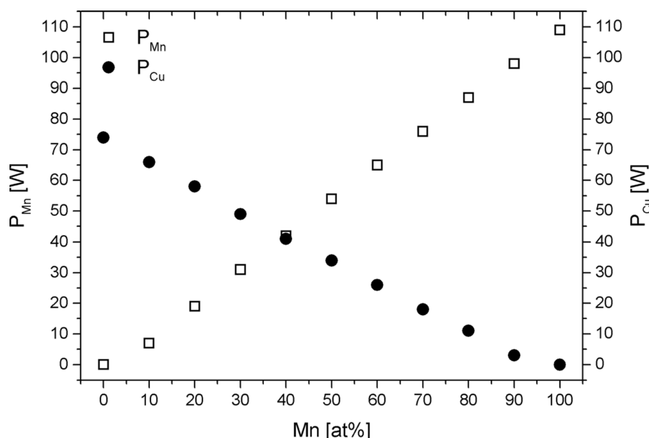

FIG. 1. Mn content of the Cu-Mn films as a function of the magnetron powers.

A. Modelling of the resistivity

The resistivity of the samples was modelled by combining the Mathiessen's rule and the Mayadas-Shatzkes[11] model in order to understand the scattering contribution of solute atoms and grain boundaries. As a general approach to describe the resistivity of a bulk material (ρ_0) the Matthiessen's rule can be used: $\rho_0 = \rho_T + \rho_I$, where ρ_T is the temperature dependent part of the resistivity and ρ_I is the residual resistivity. The latter one has a total resistivity which is the sum total of different scattering mechanisms. Generally, in thin film systems, surface- and surface-roughness scattering, solute scattering and grain boundary scattering all should be taken into account.

In the case of the Cu-Mn samples the surface and surface roughness scattering have negligible contribution to the resistivity due to the high (1 μm) thickness of the films compared to the mean free path of electrons (l_0). Thus, in the present investigation, the solute and the grain boundary scattering give significant contributions to the residual resistivity.

The solute scattering can be described by Nordheim's rule: $\rho_S = Ax(1-x)$, where x is the atomic fraction of Mn in the alloy and A is the Nordheim's coefficient. The resistivity arising from scattering at grain boundaries, however, cannot be expressed as a component in Matthiessen's rule, since it depends not only on the angle between the incident and scattered electron wave vectors, but also, on the orientation of the grain boundary as well. This contribution can be taken into account according to the Mayadas-Shatzkes model:[11]

$$\rho = 3\rho_0 \left[\frac{1}{3} - \frac{\alpha}{2} + \alpha^2 - \alpha^3 \ln\left(1 + \frac{1}{\alpha}\right)\right]^{-1}, \tag{1}$$

where ρ is the measurable resistivity of the sample, $\alpha = l_0/d \times r/(1-r)$, ρ_0 is the bulk resistivity, l_0 is the electron mean free path, d is the grain size, and r is the grain boundary reflection coefficient ($0 \leq r \leq 1$).

In our model, the electron mean free path l_0 was calculated by means of the Hall coefficient in the case of pure Mn and Cu-Mn solid solutions. For determining l_0 in solid solutions, the rule of mixture values for the electron density n were also used. The grain size d, as well as the composition interval, where the temperature dependent part of the resistivity ρ_T varies linearly with composition, were estimated from TEM images and r was chosen to give a best fit to the measured data.

III. RESULTS AND DISCUSSION

A. Electrical properties of Cu-Mn alloy films

Figure 2 shows the specific resistivity of Cu-Mn films measured over the whole composition range. For the resistivity of the pure Cu film we obtained 1.7 $\mu\Omega$ cm, while, for pure Mn, the value was 174 $\mu\Omega$ cm (Table I). The curve increases monotonously in the range of 0–80 at. % Mn content with a maximum at 80 at. % Mn corresponding to 205 $\mu\Omega$ cm.

[This article is copyrighted as indicated in the article. Reuse of AIP content is subject to the terms at: http://scitation.aip.org/termsconditions. Downloaded to] IP: 148.6.78.172 On: Thu, 04 Sep 2014 14:30:22

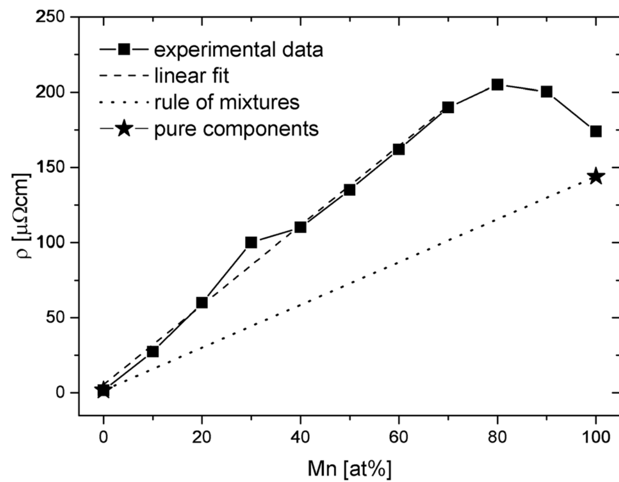

FIG. 2. Composition dependence of specific resistivity of Cu-Mn alloy films. The dotted line shows the expected behaviour for the mixture of pure components.

There is also a local maximum at the point corresponding to 30 at. % Mn.

For comparison, the line connecting the resistivity values of the pure bulk Cu and Mn ($\rho_{Cu_{bulk}} = 1.678\,\mu\Omega\,cm$,[13] $\rho_{Mn_{bulk}} = 144\,\mu\Omega\,cm$[14]) is drawn in Fig. 2. This corresponds to the rule of mixtures, i.e., to the expected variation of resistivity with composition when the components do not interact with each other and only thermal scattering contributes.[15] The fact, that the measured curve exceeds the rule of mixtures line over the entire composition interval suggests that the constituent components of Cu-Mn films can form either a solid solution, an intermetallic compound, an amorphous structure, or, a mixture of these. Some structural aspects of these interactions were reported in our previous study.[10] The boundaries between different phase regions can be evaluated from the resistivity curve in Fig. 2 by using the basic principle that changes in composition, morphology and phase change the physical properties of the materials. Consequently, the alterations in resistivity slope can designate different phase regions in the system. According to this, phase boundaries are expected around 20, 40, 70, and 80 at. % Mn content.

The temperature dependence of the resistance (R(T)) was also measured. Fig. 3 shows R(T) for Cu-Mn alloy films with different Mn content normalized to 300 K. The variation of resistance with temperature for the pure Cu film is much stronger than that for the pure Mn film (Fig. 3(a)). Alloying Cu with Mn (already at 10 at. %) significantly reduces the T dependence of R(T) (Fig. 3(b)) and makes the R(T) of alloys close to that of pure Mn. This is reflected in the TCR values as well (Fig. 4.).

The TCR of pure Cu is high (close to the bulk value[16]), while the TCR of alloy films varies remaining close of the pure Mn value. The deviation of the R(T) curves of the alloys from that of the pure Mn is not large and they look more or less similar to each other. However, the measurement of even such minor differences between them can provide useful information which can be correlated with the relevant structural data.

The film containing 10 at. % Mn shows monotonously increasing R(T) behaviour with a linear dependence in the 200–300 K interval. The corresponding positive TCR implies a metallic type of conductivity. A similar behaviour of the resistivity has been reported by Wu *et al.*[9] in the 0–10 at. % Mn concentration range of Cu-Mn alloys. The 20 at. % Mn curve, however, decreases in the 200–300 K interval. This tendency continues up to 70 at. % Mn and with increasing Mn content the slope becomes more and more negative. This is also represented in the behaviour of TCR as seen in Fig. 4.

TABLE I. Summary of the specific resistivity and TCR measured at 293 K of Cu-Mn films.

Mn (at. %)	0	10	20	30	40	50	60	70	80	90	100
ρ ($\mu\Omega$cm)	1.7	29	59	97	108	137	165	190	205	200.3	174
TCR 10^{-5} (1/K)	399	2.72	−8.39	−6.9	−23.3	−37.7	−41.5	−45.3	−30.8	−6.32	3.8

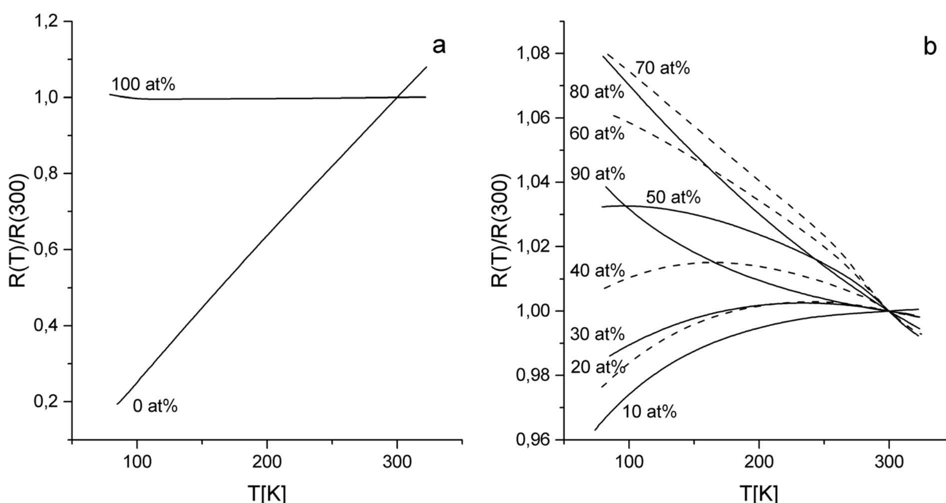

FIG. 3. The temperature dependence of normalized resistance of pure Cu and Mn films (a) and Cu-Mn alloy films with different Mn content (b). Composition of samples is indicated in at. % Mn. (The measurements were performed by 1 K steps.)

[This article is copyrighted as indicated in the article. Reuse of AIP content is subject to the terms at: http://scitation.aip.org/termsconditions. Downloaded to] IP: 148.6.78.172 On: Thu, 04 Sep 2014 14:30:22

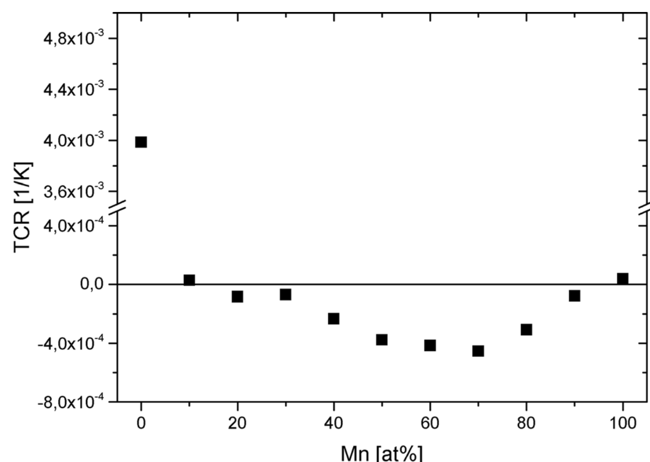

FIG. 4. Composition dependence of TCR calculated at 293 K.

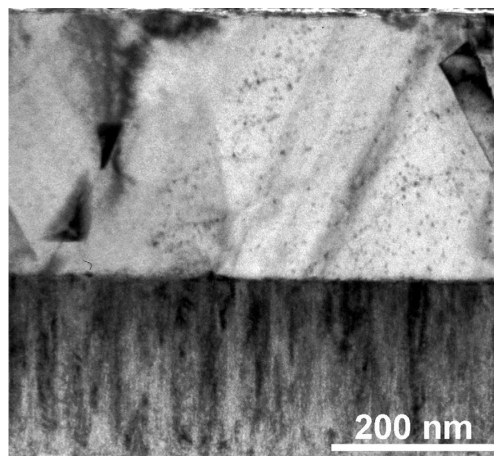

FIG. 6. Cross-sectional TEM image of pure Cu (top) and pure Mn (bottom) layer deposited onto each other. (The dark dots on the Cu layer are ion milling artefacts.)

At 80 at. % Mn content these trends reverse; the R(T) curves become concave, their value and slope decrease and approach that of the pure Mn film. The TCR of these alloys is negative and tends to the TCR value of pure Mn with increasing Mn content. The negative TCR can be attributed to the presence of disordered structures with weakly localized electrons and very high frequency of scattering which results in lower conductivity.[17–19] This correlates well with the observation of our earlier work, where amorphous structure was found in the middle of the composition range.[10]

A study of the temperature dependence of the negative TCRs can reveal details of the electronic behaviour and structural differences in these films. Two types of TCR(T) curves were obtained (Fig. 5). Between 40 and 60 at. % Mn content the TCR curves show a decreasing character with increasing temperature (Fig. 5(a)) while at 70 and 80 at. % Mn content they are less temperature dependent (Fig. 5(b)). This dissimilarity between the behaviour of TCR(T) suggests that there should be a structural difference in the corresponding films. In all TCR(T) curves a local minimum (Fig. 5) is also observed in the ~270–310 K temperature interval presumably caused by a magnetic transition. Gibbs[20] and Chouhan[21] showed in Cu-Mn alloys a transition from paramagnetic to a mixture of spin glass and antiferromagnetic states occurring below 200 K. A similar transition can be assumed in our samples, though the critical temperatures are higher. The structural differences between amorphous thin film and polycrystalline bulk samples can cause this kind of shift. The composition dependence of the transition temperature (Fig. 5) still obeys the same tendency as observed by Gibbs[20] and Chouhan.[21]

B. Structure of the films

As revealed by electrical measurements, the Cu-Mn system has several phase intervals as a function of composition. The characteristic morphology and phase state of these structures was investigated by cross sectional TEM. Fig. 6 shows an overall view of the pure Cu and Mn layer deposited on top of each other. One can see a significant difference between the morphology of the two layers. The pure Cu film (upper part of Fig. 6) has a substantially larger grain size. Its column width is equal to the film thickness which corresponds to columnar growth in zone II according to the general model of the morphological development of thin films.[22] Consequently, at higher thickness, e.g., 1 μm, also the grain size is around 1 μm. The pure Mn film has much narrower columns corresponding to zone I morphology with a column diameter around 15 nm.

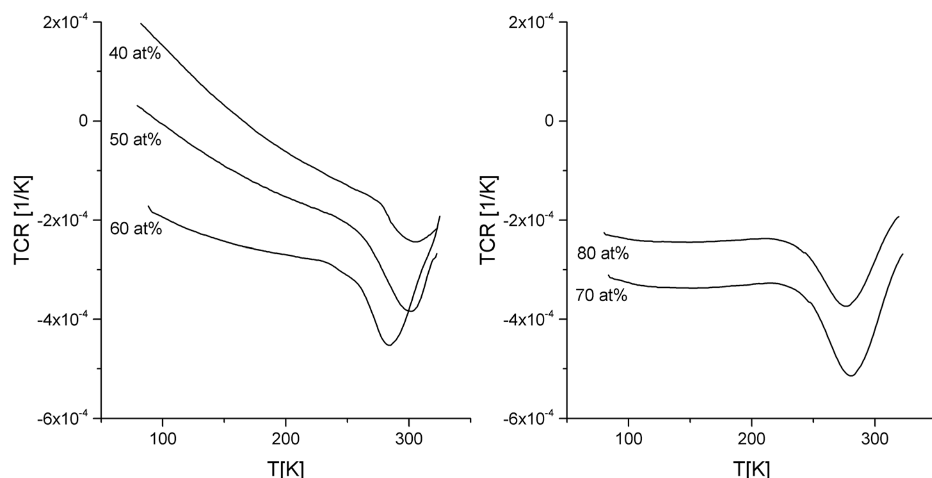

FIG. 5. Temperature dependence of TCR of 40–80 at. % Mn samples.

[This article is copyrighted as indicated in the article. Reuse of AIP content is subject to the terms at: http://scitation.aip.org/termsconditions. Downloaded to] IP: 148.6.78.172 On: Thu, 04 Sep 2014 14:30:22

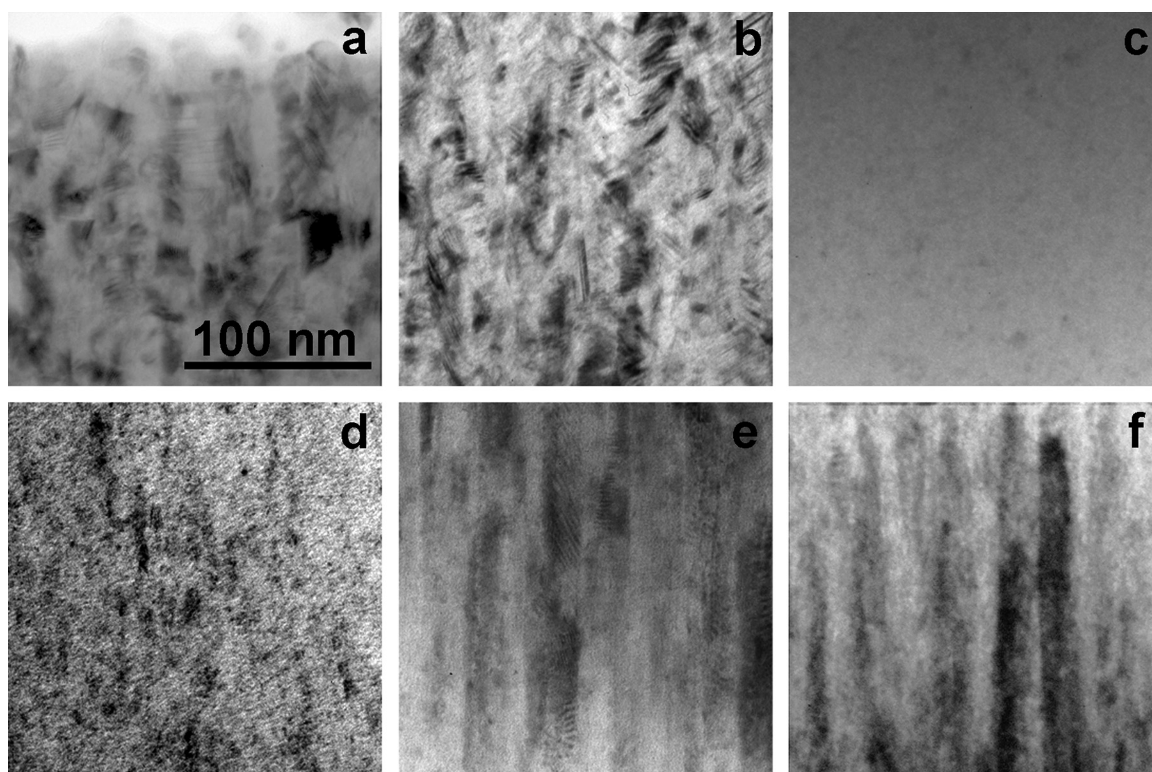

FIG. 7. Morphology of Cu-Mn alloy films with 10 at. % (a), 20 at. % (b), 60 at. % (c), 80 at. % (d), 90 at. % (e) Mn content and pure Mn film (f) revealed by cross-sectional TEM.

Fig. 7 shows the characteristic structure of Cu-Mn alloy films of each phase interval revealed by electrical measurements. The characteristic diffraction patterns of the three phase-types are shown in Fig. 8. The alloys grow with a similar morphology essentially to that of pure Mn; however, their grain size varies with the Mn content. In addition, in the middle of the alloy concentration range, an essentially different structure appears which is not expected according to the equilibrium phase diagram.[10,23,24] In this interval, between 40 and 70 at. % Mn content, the layers do not show any crystalline structure and the diffraction peaks are broad indicating amorphous structure (Figs. 7(c) and 8(b)).

In Figs. 7(b) and 7(d), it is observable that the columns are not clear and do not extend through the whole thickness of the film as would be expected in the case of a single-phase structure[22] like pure Mn and the 10 at. % Mn content film (Figs. 7(a) and 7(f)). The 10 at. % Mn layer has even clearer and longer columns (though we have some artefacts in Fig. 7(a) coming from the thinning method) than those of the layers containing 20 and 80 at. % Mn. The columns, which are much shorter than the film thickness, imply that their growth is hindered during the film development and new columnar grains start growing on their surfaces. The phenomenon is referred to as repeated nucleation[25] and is attributed to the formation of a thin covering layer on the growth surface. The phase of the covering layer is different from the phase of the columns and it forms from the condensed species which are not being incorporated into the crystal structure. The grains exhibit fcc structure in copper-rich alloys and α-Mn structure in Mn-rich alloys as indicated by Figs. 8(a) and 8(c), while the covering layers do not add reflections to the diffraction patterns.

To obtain structural information on this covering layer in films showing repeated nucleation, higher magnification and phase contrast imaging conditions were used. The reversal of grain boundary contrast between under- and over focused

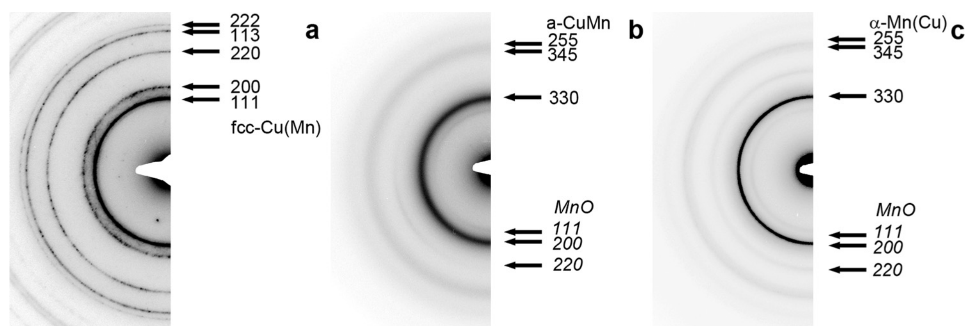

FIG. 8. The diffraction patterns of Cu-based solid solution (20 at. % Mn) (a), amorphous structure (60 at. % Mn) (b) and Mn-based solid solution (80 at. % Mn) (c). (MnO is an artefact, located on the surface of the ion-milled samples.)

[This article is copyrighted as indicated in the article. Reuse of AIP content is subject to the terms at: http://scitation.aip.org/termsconditions. Downloaded to] IP: 148.6.78.172 On: Thu, 04 Sep 2014 14:30:22

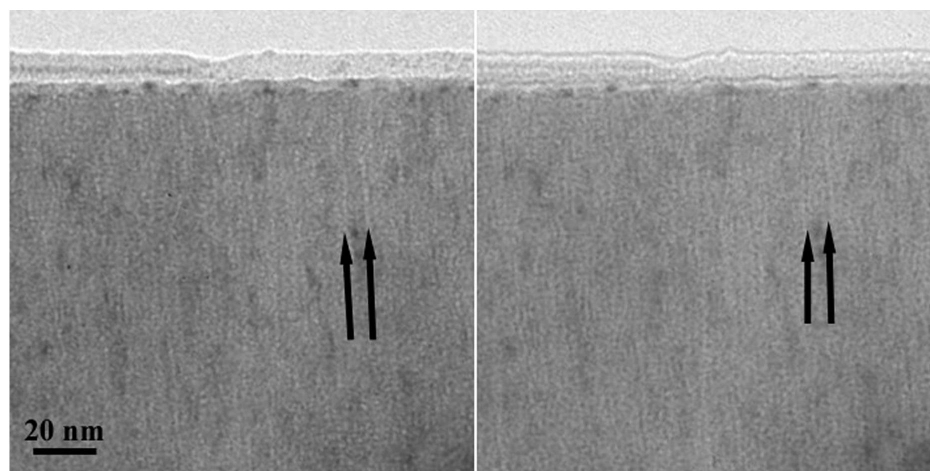

FIG. 9. Cross-sectional TEM image of Cu-Mn sample containing 80 at. % Mn. Image taken at under- (a) and at over-focused (b) conditions.

images (Figs. 9(a) and 9(b), respectively) suggests the presence of a second, less dense phase in them. In general, for similar compositions, the density of the amorphous phase is lower than that of the crystalline. Accordingly, this can be interpreted as the detection of an amorphous layer in the grain boundaries. As a consequence these films should be considered two-phase alloys. This is in good agreement with the TCR measurement, where an amorphous fraction in the structure of the films was assumed. On this basis the morphology of the two phase films can be imagined as a thin amorphous layer surrounding the crystalline grains as illustrated in Fig. 10.

Our observations testify that the transition from the two-phase crystalline to single-phase amorphous structure is rather abrupt especially in the Cu-rich alloys. According to our earlier results,[10] Cu can form supersaturated solution up to ~35 at. % Mn, however, the degree of supersaturation depends on the Mn content of the alloy. The crystalline grains of the two-phase films nucleate from the mixture of component atoms in the initial stages of growth. The higher the Mn content, the more supersaturated the nucleating crystallites become. However, the nucleation conditions of the crystalline alloy phase significantly change at the composition of the highest supersaturation (at ~35 at. % Mn). At this composition a crystalline Mn phase should also nucleate, according to the phase diagram. Nevertheless, this cannot occur probably due to the extremely large unit cell of the α-Mn phase and the kinetic limitations during film growth assignable to deposition conditions. Thus phase separation cannot occur and an amorphous structure develops. The transition from two-phase crystalline to single-phase amorphous films takes place in a similar way in Mn-rich alloys as well.

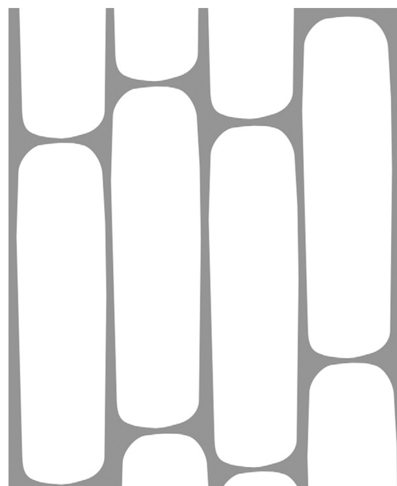

FIG. 10. Schematic view of the two phase region of Cu-Mn system (crystals are bright, the amorphous grain boundaries are grey).

The lateral grain sizes and corresponding phase state derived from the TEM images are listed in Table II.

C. Modelling of the resistivity

By exploring the connection between the established phases and the measured conductivity a model has been worked out. Composition of the resistivity curve from its components according to different scattering mechanisms shows how characteristic these mechanisms are for the observed phases and how these components are dependent on film composition. For the basic scattering mechanisms of the rather complex system, the following composition dependences can be considered.

The solute scattering of solid solutions is usually described by a parabolic curve. In the Cu-Mn thin film system this approach can also be used, as the solute content is continuous for all compositions. The Nordheim's coefficient of the curve can be estimated from the measured resistivity by linear approximation at low Mn concentrations, giving $A = 276\ \mu\Omega\,\text{cm}$. This value is in good accordance with $A = 249\ \mu\Omega\,\text{cm}$ measured on bulk wire samples by Otter.[26]

The simplest description of the thermal scattering could be the linear interpolation between the resistivity of pure components. This would be a valid approximation for the structure comprising a mixture of crystallites of the pure components. However, there are solid solutions at the two ends of the concentration regions, where the effect of solutes has already been accounted for by the solute scattering component. At these concentrations the thermal component will be expected to be independent of composition. Hence, the

[This article is copyrighted as indicated in the article. Reuse of AIP content is subject to the terms at: http://scitation.aip.org/termsconditions. Downloaded to] IP: 148.6.78.172 On: Thu, 04 Sep 2014 14:30:22

TABLE II. Data used for calculating grain boundary scattering in Cu-Mn films.

at. % Mn	0	10	20	30	40	50	60	70	80	90	100
Phase type	Single-phase		Two-phase		Single-phase			Two-phase		Single-phase	
d (nm)	1000	30	15	15	—	—	—	10	10	10	15
ρ_0/ρ (-)	0.982	0.967	0.764	0.815	1	1	1	0.891	0.864	0.842	0.828
l_0 (nm)	39	2	1.5	1	0.5	0.5	0.5	0.5	0.5	0.5	0.5
α (-)	0.012	0.023	0.216	0.157	0	0	0	0.084	0.108	0.129	0.144
r (-)	0.24	0.27	0.69	0.76	—	—	—	0.63	0.68	0.72	0.81

linear interpolation for thermal scattering starts at the end of solid solution regions.

By summing up the resistivity contributions of the two scattering mechanisms the reliability of the approaches used can be shown (Fig. 11) as it describes the measured resistivity quite satisfactorily. At 10 at. % Mn content the same value of 25 $\mu\Omega$cm is obtained as by Otter[26] and Domenicali[27] for a wire sample. The curve fits well to the measured one also in the amorphous region (40–60 at. % Mn), where no other scattering mechanisms are assumed. The sum underestimates the resistivity of the film at 20 and 30 at. % Mn and from above 70 at. % Mn (Fig. 11). The difference can be attributed to scattering at grain boundaries, which was calculated (Eq. (1)) by fitting the experimental data. For the calculation of the grain boundary reflection coefficient (r) grain size (d) and electron mean free path (l_0) had to be determined at each composition.

Grain size was obtained from cross-sectional TEM images by measuring the diameter of the columnar grains. For pure Cu l_0 was taken from the literature[11,13] to be around 40 nm. For Mn, it was calculated from its Hall coefficient R_H, which is $-0.93 \times 10^{-4} \mathrm{cm}^3/\mathrm{C}$.[28] l_0 can be expressed as $l_0 = v_F \times \tau$ where $v_F = \hbar/m \times (3\pi^2 n)$ is the Fermi velocity and $\tau = m/(\rho_0 e^2 n)$ is the relaxation time. The electron density $n = 1/(R_H \times e)$ can be calculated from the Hall coefficient. In the solid solutions l_0 was determined by using the rule of mixture values for n electron density (Table II). The resulting r values obtained from these data are listed in Table II.

The grain boundary reflection coefficients (r) are plotted in Fig. 12. The r values of pure Cu and 10 at. % Mn films are close to each other and are 0.24 and 0.27, respectively. Mayadas *et al*. calculated a similar reflection coefficient for Cu samples.[11] Films in the 40–70 at. % Mn interval exhibit no grain boundaries according to TEM measurements, thus no r was calculated here. In the two-phase (20–40 and 70–90 at. % Mn) regions the r values fall between 0.6 and 0.8 indicating the high scattering effect of the grain boundaries. This suggests the presence of a special, less conductive grain boundary structure in these films providing further evidence of the existence of an amorphous grain boundary layer, as illustrated in Fig. 10. For pure and 90 at. % Mn content films the calculated r values are unexpectedly high. The single-phase nature of these films would imply smaller r compared to two-phase films. However, in the high Mn content samples d and l_0 are small resulting a higher r. Beside this, further TEM investigation of pure Mn films revealed the fragmentation of Mn columns, a result which still needs further confirmation. Utilizing these later investigations a smaller r would result, but the influence also of further scattering mechanisms cannot be excluded.

Apart from leaving the question concerning the grain boundary properties of Mn based solid solutions open, the model gives strong evidence for the maxima of resistivity in the two-phase regions. Generally, in a binary system, the resistivity of the two-phase structure is expected to be smaller than that for the corresponding solid solution. However, if the two phases form a particular morphology, new scattering

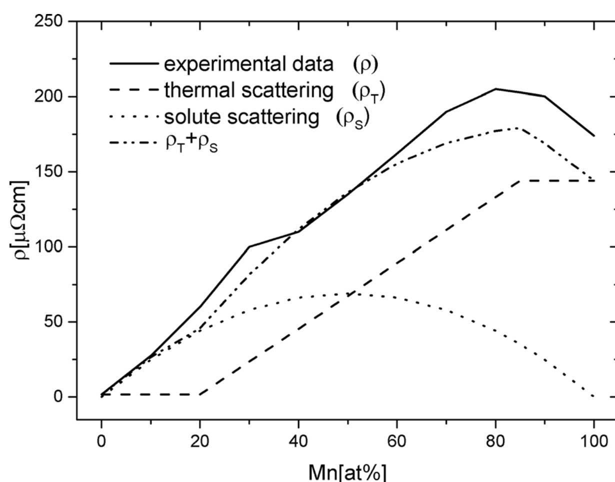

FIG. 11. The calculated contribution of thermal- and solute-scattering to the resistivity and their sum compared with the experimental data as a function of Mn content.

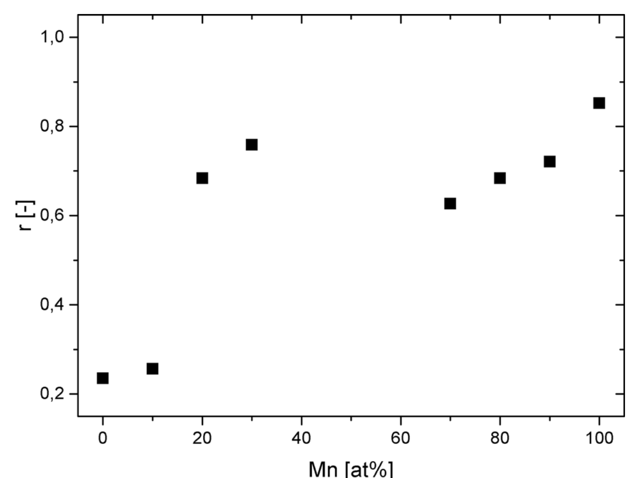

FIG. 12. Grain boundary reflectivity coefficient (r) as a function of Mn content. The grain boundary scattering is significant when r is high.

[This article is copyrighted as indicated in the article. Reuse of AIP content is subject to the terms at: http://scitation.aip.org/termsconditions. Downloaded to] IP: 148.6.78.172 On: Thu, 04 Sep 2014 14:30:22

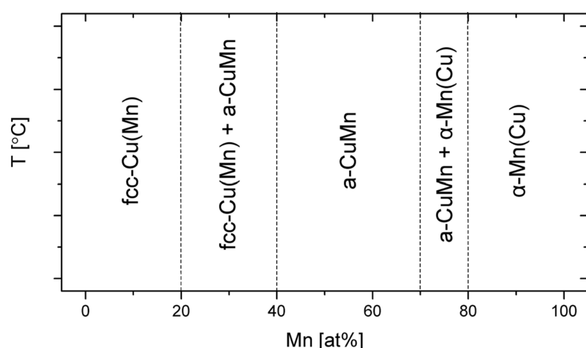

FIG. 13. Phase diagram of DC magnetron sputtered Cu-Mn alloy films suggested around room temperature.

mechanisms can become effective resulting in an increase of resistivity. The presented model confirms the special arrangement of the phases in the Cu-Mn system. The amorphous grain boundary layer around the crystalline Cu- or Mn-rich solid solution grains results in an additional contribution to the grain boundary scattering mechanisms through higher r values. With the help of this contribution, the resistivity maxima in the two-phase regions can be understood.

By understanding the unusual composition dependence of the resistivity of Cu-Mn films and taking into account the TEM results it is possible to specify the location of phase regions in the system, as shown schematically in Fig. 13.

IV. SUMMARY

Cu-Mn alloy thin films were deposited by DC magnetron sputtering at room temperature. The specific resistivity of films measured over the whole composition range shows monotonous increase in the 0–80 at. % Mn interval with a 205 $\mu\Omega$ cm maximum at 80 at. % Mn. There is also a local maximum at the point corresponding to 30 at. % Mn. The alterations in the slope of the resistivity curve designated the different phase regions in the system. According to this, boundaries of phase intervals are identified at 20, 40, 70, and 80 at. % Mn content. A correlation was found between these intervals and the structure of the corresponding films. Cross-sectional TEM investigations revealed that, in the 0–20 at. % and 80–100 at. % Mn intervals, the films exhibited columnar, single-phase structure. Also a single-phase but amorphous structure exists at the 40–70 at. % Mn interval, whereas, for 20–40 at. % and 70–80 at. % Mn content, two-phase structures were found. The two-phase nature of these films was confirmed not only from the structural data but also by TCR measurements and by modelling of the scattering mechanisms in the system. Negative TCR values indicate the existence of a non-metallic, amorphous component, while the calculated high grain boundary reflection coefficients suggest its alignment along the grain boundaries. The proposed model provides an explanation for the resistivity maxima indicating that, in binary systems, the special arrangement of the two phases introduces new scattering mechanisms resulting in an increase in resistivity. We suppose that the model can be applied for a broader class of composite thin films.

Our results also suggest that, for integrated device applications, other composition ranges are worth consideration in addition to low Mn content solid solutions. The lack of grain boundaries makes amorphous films viable for the formation of a thin, conformal barrier layer, and, moreover, their resistivity compares well with that for the recently used Ta/TaN layers (140 $\mu\Omega$ cm (Ref. 29)).

ACKNOWLEDGMENTS

The authors acknowledge the financial support of the Hungarian Academy of Sciences under the Grant No. of OTKA-K81808. F. Misják also acknowledges the support by the János Bolyai Research Scholarship of the Hungarian Academy of Sciences. P. Lobotka acknowledges the financial support from the Grant No. APVV-0593-11.

[1] J. Koike and M. Wada, Appl. Phys. Lett. **87**, 041911 (2005).
[2] J. Koike, M. Haneda, J. Iijima, Y. Otsuka, H. Sako, and K. Neishi, J. Appl. Phys. **102**, 043527 (2007).
[3] M. Haneda, J. Iijima, and J. Koike, Appl. Phys. Lett. **90**, 252107 (2007).
[4] K. Matsumoto, K. Neishi, H. Itoh, H. Sato, S. Hosaka, and J. Koike, Appl. Phys. Express **2**, 036503 (2009).
[5] J. M. Ablett, J. C. Woicik, Z. Tőkei, S. List, and E. Dimasi, Appl. Phys. Lett. **94**, 042112 (2009).
[6] J. G. Lozano, S. Lozano-Perez, J. Bogan, Y. C. Wang, B. Brennan, P. D. Nellist, and G. Hughes, Appl. Phys. Lett. **98**, 123112 (2011).
[7] C. H. Liu, W. Liu, Y. H. Wang, Y. Wang, Z. An, Z. X. Song, and K. W. Xu, Microelectron Eng. **98**, 80 (2012).
[8] J. Iijima, Y. Fujii, K. Neishi, and J. Koike, J. Vac. Sci. Technol. B **27**, 1963 (2009).
[9] C.-Y. Wu, C.-T. Wu, W.-H. Lee, S.-C. Chang, and Y.-L. Wang, J. Alloys Compds. **542**, 118 (2012).
[10] Z. Czigány, F. Misják, O. Geszti, and G. Radnóczi, Acta Mater. **60**, 7226 (2012).
[11] A. F. Mayadas and M. Shatzkes, Phys. Rev. B **1**, 1382 (1970).
[12] Á. Barna, G. Radnóczi, and B. Pécz, *Preparation Techniques for Transmission Electron Microscopy* (VHC, Cambridge, 1997), Vol. 3, p. 751.
[13] W. Zhang, S. H. Brongersma, O. Richard, B. Brijs, R. Palmans, L. Froyen, and K. Maex, Microelectron Eng. **76**, 146 (2004).
[14] P. D. Desai, H. M. James, and C. Y. Ho, J. Phys. Chem. Ref. Data **13**, 1131 (1984).
[15] Z. Fan, P. Tsakiropoulos, and A. P. Miodownik, J. Mater. Sci. **29**, 141 (1994).
[16] V. V. R. N. Rao, S. Mohan, and P. J. Reddy, J. Phys. D **9**, 89 (1976).
[17] K. Pekala and D. Oleszak, Rev. Adv. Mater. Sci. **18**, 197 (2008).
[18] V. F. Gantmakher, JETP Lett. **94**, 626 (2011).
[19] J. H. Mooij, Phys. Status Solidi A **17**, 521 (1973).
[20] P. Gibbs, T. M. Harders, and J. H. Smith, J. Phys. F **15**, 213 (1985).
[21] R. K. Chouhan and A. Mookerjee, J. Magn. Magn. Mater. **323**, 868 (2011).
[22] I. Petrov, P. B. Barna, L. Hultman, and J. E. Greene, J. Vac. Sci. Technol. A **21**, S117 (2003).
[23] See http://resource.npl.co.uk/mtdata/phdiagrams/cumn.htm for National Physical Laboratory.
[24] H. Okamoto, J. Phase Equilib. **19**, 180 (1998).
[25] P. B. Barna and M. Adamik, Thin Solid Films **317**, 27 (1998).
[26] F. A. Otter, J. Appl. Phys. **27**, 197 (1956).
[27] C. A. Domenicali and E. L. Christenson, J. Appl. Phys. **32**, 2450 (1961).
[28] D. E. Gray, *AIP Handbook* (McGraw-Hill, New York, 1972).
[29] M. Haneda, N. Ohtsuka, H. Kudo, T. Tabira, M. Sunayama, N. Shimizu, H. Ochimizu, and A. Tsukune, Jpn. J. Appl. Phys. **49**, 05FA01 (2010).

[This article is copyrighted as indicated in the article. Reuse of AIP content is subject to the terms at: http://scitation.aip.org/termsconditions. Downloaded to] IP: 148.6.78.172 On: Thu, 04 Sep 2014 14:30:22